Materials Research Bulletin 62 (2015) 184–191

Contents lists available at ScienceDirect

Materials Research Bulletin

journal homepage: www.elsevier.com/locate/matresbu

Synthesis of MoO_3 nanoparticles for azo dye degradation by catalytic ozonation

Arumugam Manivel [a], Gang-Juan Lee [a], Chin-Yi Chen [b], Jing-Heng Chen [c], Shih-Hsin Ma [c], Tzzy-Leng Horng [d], Jerry J. Wu [a,*]

[a] Department of Environmental Engineering and Science, Feng Chia University, Taiwan
[b] Department of Material Science and Engineering, Feng Chia University, Taiwan
[c] Department of Photonics, Feng Chia University, Taiwan
[d] Department of Applied Mathematics, Taiwan

ARTICLE INFO

Article history:
Received 2 August 2014
Received in revised form 29 October 2014
Accepted 4 November 2014
Available online 6 November 2014

Keywords:
Molybdenum trioxide
Catalytic ozonation
Orange II dye
Sonochemical synthesis
Nanoparticles
Microwave synthesis

ABSTRACT

One-dimensional molybdenum trioxide nanostructures were prepared in three different approaches, including thermal, microwave, and sonochemical methods. The physicochemical properties of the obtained MoO_3 nanoparticles were investigated by diffused reflectance spectroscopy, X-ray diffraction analysis, field emission scanning electron microscopy, high resolution transmission electron microscopy, and Brunauer–Emmett–Teller surface area analysis. Among the methods as investigated, sonochemical synthesis gave well-dispersed fine MoO_3 nanoparticles compared with the other approaches. All the synthesized MoO_3 nanostructures were examined for the catalytic ozonation to degrade azo dye in aqueous environment. Different performances were obtained for the catalyst prepared in different methods and the catalytic efficiencies were found to be the order of sonochemical, microwave, and then thermal methods. The sonochemical MoO_3 catalyst allowed the total dye removal within 20 min and its good performance was justified according to their higher surface area with higher number of active sites that provide effective dye interaction for better degradation.

1. Introduction

In recent years, numerous inspired schemes and pathways have been developed for the synthesis of transition metal oxide nanomaterials. These materials have been the focus of passionate research because of their potential applications in diverse fields of technology [1–3]. Among the intriguing transition-metal oxides, molybdenum oxides and its derivatives are extensively attractive due to their unique structural and optical properties [4–7]. Although molybdenum has oxidation states ranging from +2 to +6, oxides exist mainly in two forms, such as molybdenum (IV) and molybdenum (VI) oxide [8]. The existence of metal-like electronic conductivity of molybdenum (IV) oxide has formulated them as promising materials in energy related applications [8–10]. Molybdenum (VI) oxide (MoO_3), a wide band gap *n*-type semiconductor with distinctive electrochromic, thermochromic, and photochromic properties, has been widely investigated as smart materials for catalysis [11,12], sensors [13–15], lubricants [5], lithium battery [16–18], organic solar cells [19,20], and display materials [21]. Generally molybdenum (VI) oxide exhibits in three forms, including orthorhombic (α-MoO_3), monoclinic (β-MoO_3), and hexagonal (h-MoO_3) [22–24]. The meta-stable β-MoO_3 and h-MoO_3 were intensively investigated than the thermodynamically stable α-MoO_3 due to their excellent physicochemical properties [25,26]. It is literally known that phase purity of MoO_3 relied on the adopted synthetic procedure and experimental conditions [26,27]. Considerable progresses have been accomplished recently for the size and phase controlled synthesis of MoO_3 with optimized catalytic properties [13,28]. Methods, such as flame synthesis [29], thermal evaporation [30], sputtering process [31], chemical vapor deposition [32], hydrothermal [13,21,27,33,34], infrared irradiation [35], microwave methodology [36], electrochemical process [37] and sonochemical approach [7,38], have been noted for the successful synthesis of MoO_3 nanostructures. However, the study on the synthesis of MoO_3 nanostructures in different approaches and their comparison for a catalytic process is still limited and there remains much interest. Therefore, we attempted to prepare MoO_3 nanostructures in this study by using three different methods, including hydrothermal, microwave, and sonochemical methods. This approach offers an opportunity to compare the

* Corresponding author. Tel.: +886 4 24517250x5206; fax: +886 4 24517686.
E-mail address: jjwu@fcu.edu.tw (J.J. Wu).

http://dx.doi.org/10.1016/j.materresbull.2014.11.016
0025-5408/

influence of experimental methods on physicochemical properties. In addition, their catalytic properties were examined for the heterogeneous catalytic ozonation of orange II dye. To the best of our knowledge, there is no report available for the degradation of orange II dye under MoO_3 assisted catalytic ozonation processes.

2. Methodology

2.1. Materials

Ammonium heptamolybdate tetrahydrate $(NH_4)_6Mo_7O_{24}{\cdot}4H_2O$, nitric acid, and ethanol were purchased from Merck chemicals. Orange II was purchased from Acros chemicals. All the reagents and chemicals used in this study were used as received without further purification.

2.2. Instrumental

Microwave reactions were carried out in CEM Discover microwave system (300 W) equipped with in-situ magnetic stirrer and programmable microwave exposure time and temperature. The preset profile (desired time and temperature) was followed by automatically adjusting the applied microwave power. A horn type (20 kHz SONICS sonifier) with a tip diameter of 1 cm was used for carrying out sonochemical synthesis. The X-ray diffraction (XRD) patterns were recorded using Rigaku Ultima III diffractometer (Japan) with Cu-Kα1 radiation in the scan angle range from 10° to 90°. The morphologies of the catalysts were examined by using JEOL JSM-7401F field emission scanning electron microscope (FE-SEM). Prior to FE-SEM measurements, the samples were placed on conductive carbon ink and then gold sputtering was performed. High resolution transmission electron microscopic (HR-TEM) images were recorded using JEOL JEM-2010 model. Samples for HR-TEM were prepared as follows: a small amount of samples were mixed with ethanol and ultrasonically dispersed for 5 min. A drop of this suspension was placed onto the copper grid and then drying in air. The UV–vis diffuse reflectance spectra were recorded using Shimadzu UV-2600 spectrophotometer with integrated sphere attachment and barium sulfate as a reference. The absorbance of the dye was also measured by using the same instrument with universal liquid cell attachment. In addition, the Brunauer–Emmett–Teller (BET) surface area, pore size, and pore volume of the catalysts were measured by nitrogen adsorption method using Micrometrics ASAP-2020 instrument. Prior to analysis, 0.5 g of powder was degassed at 120 °C for 15 h.

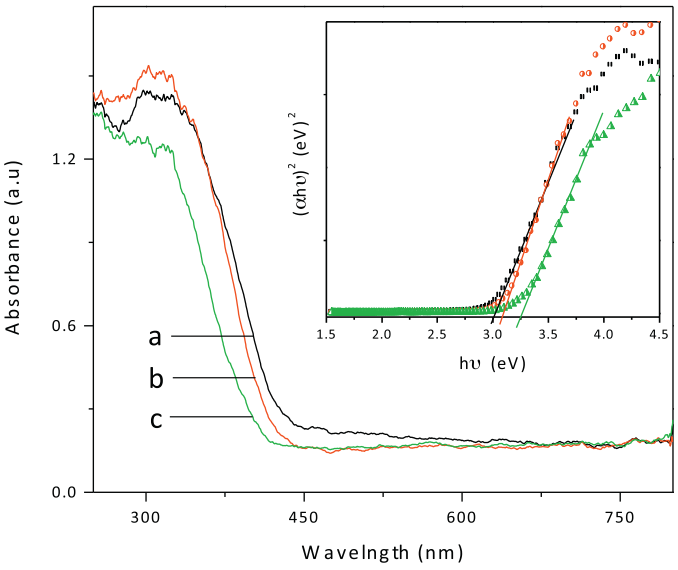

Fig. 1. Solid state UV–vis spectrum of MoO_3 nanoparticles synthesized in (a) thermal, (b) microwave, and (c) sonochemical method. Inset shows the bang gap graph obtained from UV data.

2.3. Synthesis of MoO_3 nanoparticles

MoO_3 nanoparticles were prepared according to the procedure reported in the Ref. [13,34] but with a slight modification in the current study. Briefly, 10 mL 0.2 M of ammonium heptamolybdate tetrahydrate was used in the beaker and stirred for 10 min to obtain a clear solution. Then 5 mL of concentrated HNO_3 was added drop-wise to the above solution and stirred for 10 min. This mixture was served as the common solution for all synthesized methods. For hydrothermal method, the mixture was transferred to the autoclave and heated to 100 °C for 2 h. The heating rate was maintained at 10 °C min^{-1}. After 2 h of heating, the autoclave was allowed to cool down to room temperature. The resultant mixture was centrifuged

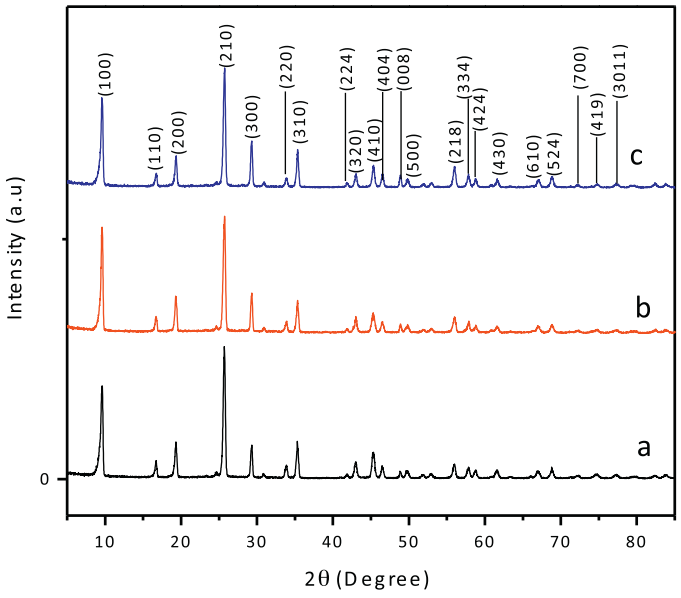

Fig. 2. X-ray diffraction patterns of MoO_3 nanoparticles prepared in (a) thermal, (b) microwave, and (c) sonochemical methods.

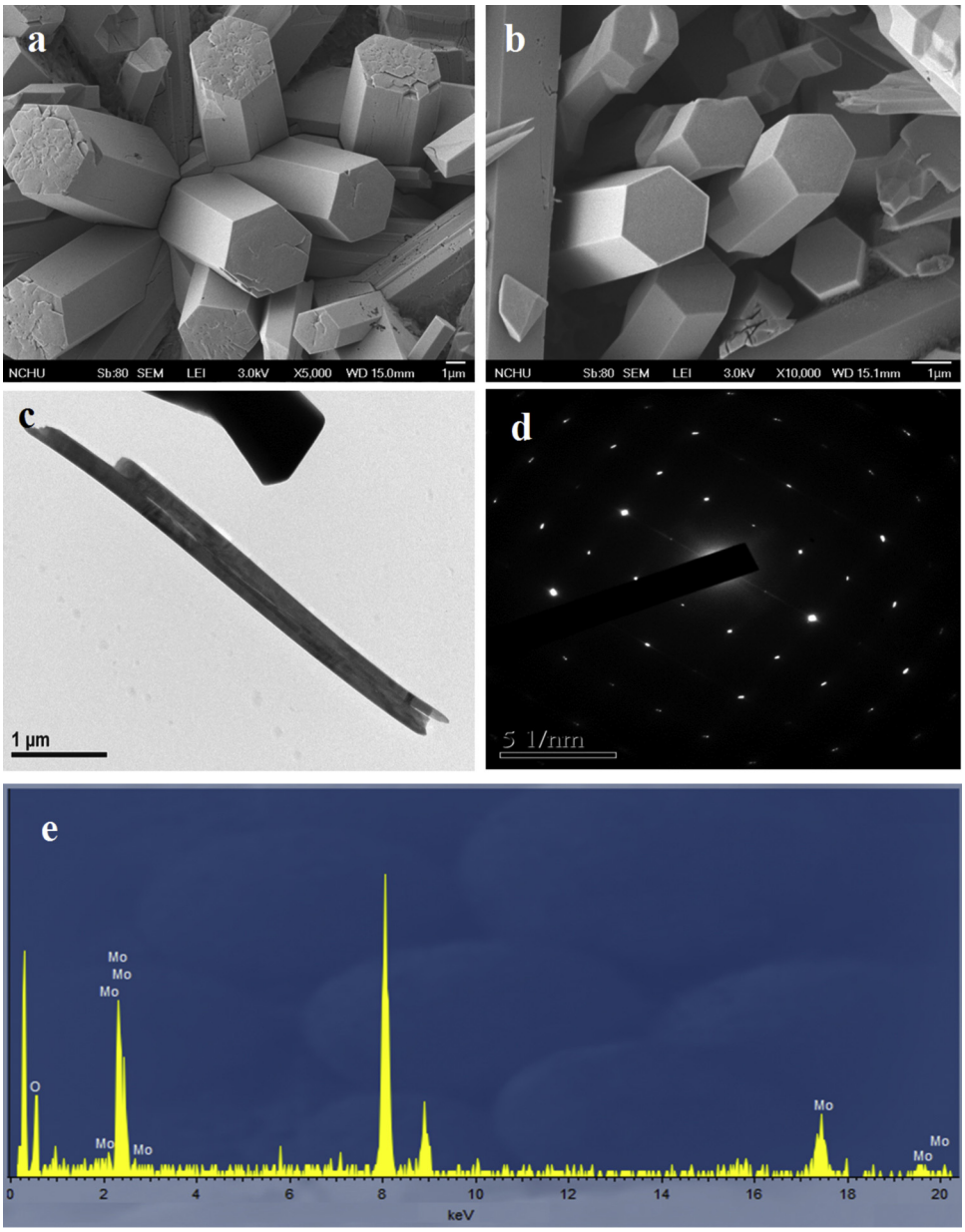

Fig. 3. (a) and (b) SEM images, (c) TEM image, (d) SAED patterns, and (e) EDS spectrum of the MoO_3 nanoparticles synthesized in thermal method.

and washed several times with water and finally washed with ethanol. The final product was dried at 70 °C in the oven for 12 h. For microwave method, freshly prepared initial solution was irradiated by the microwave for 10 min with a power of 70 W at 100 °C. Cooling was then maintained throughout experiment. The final white precipitate was filtered and washed several times with water and finally with ethanol. The final solid white powder was dried in oven for 12 h at 70 °C. For the sonochemical method, freshly prepared initial solution was sonicated in a horn type ultrasonicator for 1 h with an amplitude of 30% and pulse cycle of 55 s on and 5 s off. The final milky white solution was centrifuged and washed several times with water and finally with ethanol. The final solid white powder was dried in the oven for 12 h at 70 °C.

2.4. Evaluation of catalytic activity

A 500 mL capacity borosilicate glass reactor was used for the catalytic ozonation experiments. The degradation of orange II was carried out at ambient conditions (25 ± 2 °C) and natural pH (7.0). The amount of catalyst and orange II dye used for all the experiments was the same (250 mg per 250 mL of 1.0×10^{-4} M dye in aqueous solution). Prior to ozonation experiments, the dye solution was stirred for 30 min with the catalyst to ensure adsorption/desorption equilibrium. Ozone was purged to the dye solution through a porous fritted diffuser that can produce fairly fine bubbles with diameter less than 1 mm. Ozone was produced from pure oxygen by corona discharge using an ozone generator (ESCO). The gas flow rate was regulated at 50 mL min^{-1} by a mass flow controller (Brooks 5850E) and the inflow ozone concentration was adjusted to 5 mg L^{-1}. The gaseous ozone concentrations were determined spectrophotometrically by the absorbance of ozone measured in a 2 mm flow-through quartz cuvette at the wavelength of 254 nm. A small amount of the experimental solution was withdrawn at a regular time interval and the degradation was followed by using UV–vis spectrophotometer at the absorbance maximum around λ_{max} = 485 nm. For

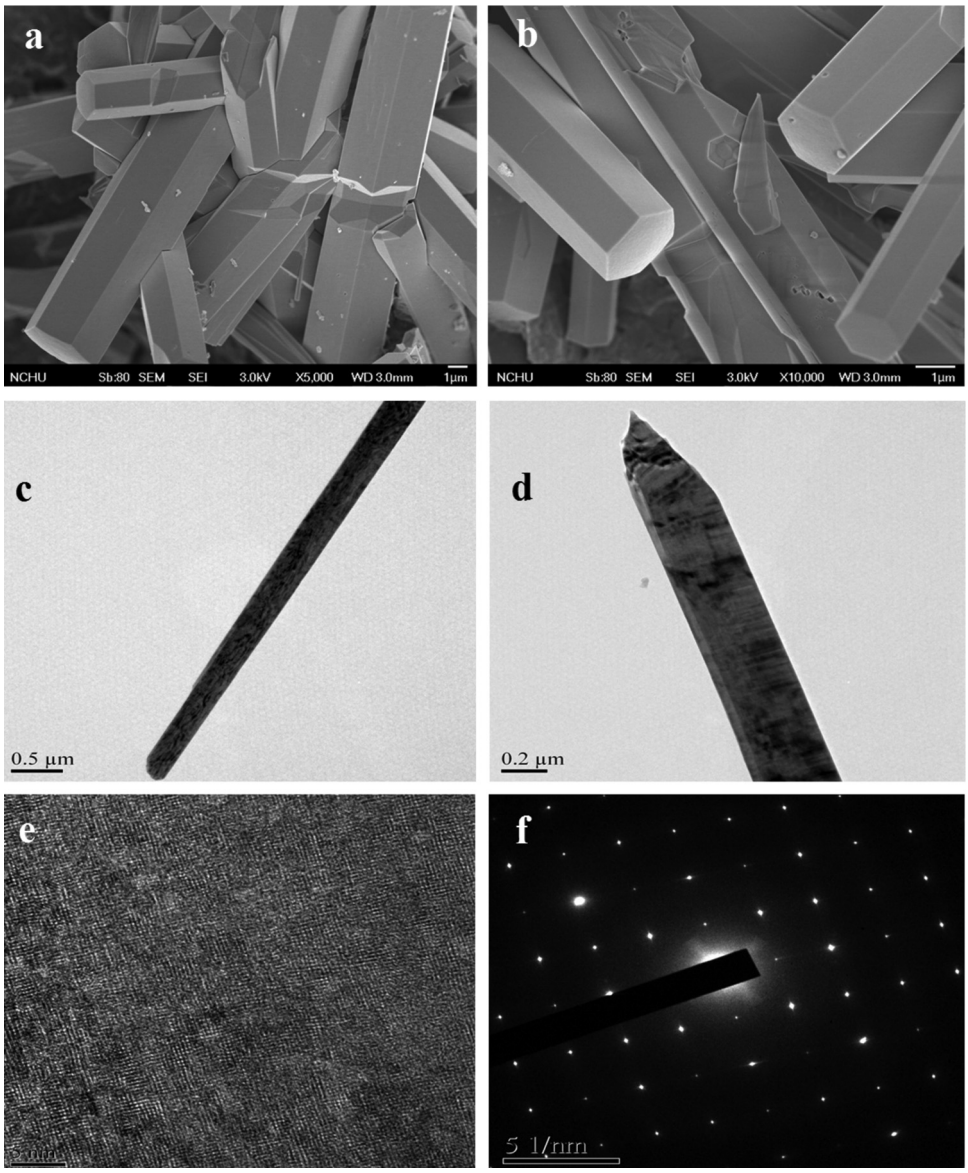

Fig. 4. (a) and (b) SEM images, (c) and (d) TEM images, (e) HR-TEM image, and (f) SAED patterns of the MoO_3 nanoparticles synthesized in microwave method.

catalytic experiments, the catalyst was removed prior to the analysis by centrifugation at 5000 rpm followed by filtration using a 0.45 μm polyvinylidene fluoride (PVDF) syringe filter. The linear relationship between $-\ln(C/C_0)$ vs. irradiation time gave the first-order degradation kinetics.

3. Results and discussion

3.1. Characterization of the MoO_3 nanoparticles

Optical properties and electronic structural features of the synthesized MoO_3 nanoparticles were analyzed by solid state UV–vis absorbance spectroscopy. Fig. 1 shows the diffused reflectance spectra (DRS) of MoO_3 nanoparticles prepared in thermal (Fig. 1a), microwave (Fig. 1b), and sonochemical (Fig. 1c) methods. Absorbance edge positions of 440 nm, 430 nm, and 410 nm were obtained for the samples prepared in thermal, microwave and sonochemical methods, respectively. Such different absorbance cut values and shift in absorbance onset values could be explained based on the well-known quantum size effect of the semiconductor nanoparticles reported elsewhere that the wavelength decreases with reduce in size. Furthermore, it also indicates that the samples prepared in different methods have dissimilar sizes.

According to the inter-band absorption theory, the absorption coefficient near the threshold vs. incident energy can be related to the following relation [39]

$$(\alpha h_v) = A_n(h_v - E_g)^n$$

where, A_n is the probability parameter for the transition and E_g is optical energy gap. The coefficient 'n' is equal to 1/2 and 2 for allowed direct transitions and indirect transitions, respectively. Since $(\alpha h_v)^{1/2}$ does not give a linear relationship, it suggests that all synthesized MoO_3 nanoparticles have a direct gap. The E_g value corresponding to direct band gap transitions can be given by,

$$(\alpha h_v)^2 = A(h_v - E_g)$$

The linear region of $(\alpha h_v)^2$ vs. h_v graph (inset of Fig. 1) was fitted and the energy gap (E_g) values were derived from the slopes of the plot. MoO_3 nanoparticles synthesized in thermal method show the

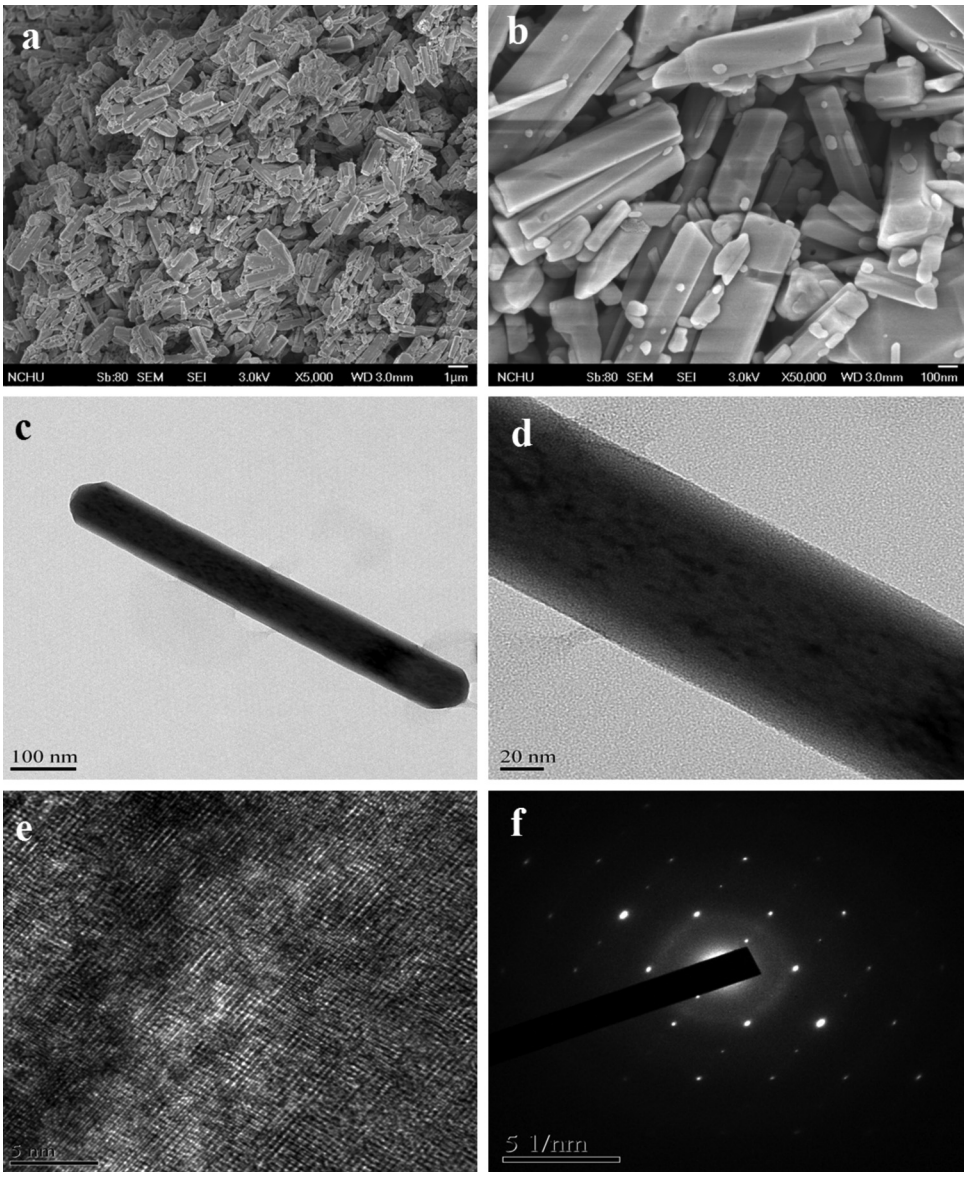

Fig. 5. (a) and (b) SEM images, (c) and (d) TEM images, (e) HR-TEM image, and (f) SAED patterns of the MoO_3 nanoparticles synthesized in sonochemical method.

energy gap of 3.05 eV, which is in accordance with the values reported literally. However, the microwave method for synthesizing MoO_3 nanoparticles gave a slight increase in energy values (3.11 eV), whereas the MoO_3 nanoparticles obtained from sonochemical method gave the highest band gap energy (3.25 eV). This could be resulted from the quantum confinement effect of smaller sonochemical product.

The phase and crystallographic structures of the synthesized MoO_3 nanoparticles were examined by X-ray diffraction (XRD) analysis. Fig. 2(a–c) shows the typical XRD patterns of the MoO_3 nanoparticles obtained using different methods. The high degree of crystallinity was confirmed from the well-defined sharp peaks and all the three spectra were found to be as similar to each other. The diffraction patterns are good in agreement with the hexagonal phase MoO_3 with lattice parameters of $a = 10.53$ Å and $c = 14.876$ Å (JCPDS card no. 21-0569, space group $P63$). No obvious diffraction patterns for other phases were found in all the three samples, indicating the phase purity of the synthesized products. The observed peak broadening is attributed to the size and strain effect. The crystallite size can be estimated from the full width half maximum (FWHM) values obtain from the predominant (0 2 1) diffraction peak at 25.7 according to the following Debye–Sherrer equation

$$D_{hkl} = \frac{k\lambda}{\beta_{hkl}\cos\theta_{hkl}}$$

where K is the shape factor (0.9), λ is the wavelength of Cu-Kα1 radiation (1.5406 Å), and θ_{hkl} is the Bragg diffraction angle. The calculated crystallite size was around 94, 86, and 64 nm for MoO_3 obtained in thermal, microwave, and sonochemical methods, respectively. Sonochemical reactions arising from acoustic cavitations phenomena [40] are the reason for the formation of relatively smaller sonochemical MoO_3.

Surface morphological changes were investigated by using scanning electron microscopy and transmission electron microscopic analyses. Fig. 3a and b shows the FE-SEM images of MoO_3 samples obtained from the thermal method. It is clearly seen that the sample consists of uniform hexagonal rod-like morphology. A representative TEM image of the sample is depicted in Fig. 3c, which obviously shows the formation of rods with few hundred nanometers thickness and few micrometers in length. Selected area electron diffraction (SAED) analysis was also conducted

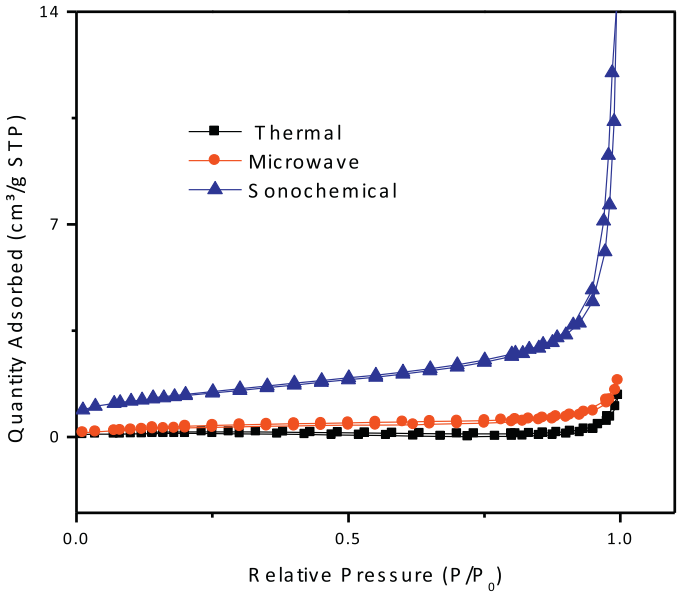

Fig. 6. BET surface area analysis of the MoO_3 nanoparticles prepared in (a) thermal, (b) microwave, and (c) sonochemical methods.

(Fig. 3d) and it shows the crystalline dotted patterns as an evident for the formed hexagonal phase. The energy dispersive X-ray spectroscopy analysis (EDS) also confirmed the elemental composition of MoO_3 and no other impurity was detected. The FE-SEM (Fig. 4a and b) and TEM analysis (Fig. 4c and d) of microwave synthesized MoO_3 nanoparticles also shows similar hexagonal rod-like morphology. However, their rod thickness was slightly decreased (200–300 nm) compared to thermal prepared MoO_3. The clear lattice fringes of MoO_3 can be observed from HR-TEM analysis. In addition, SAED patterns show crystalline dotted patterns corresponding to hexagonal MoO_3. SEM images of sonochemically synthesized MoO_3 nanoparticles are shown in Fig. 5a and b. Comparing to SEM images of thermal and microwave synthesized MoO_3 when ultrasound irradiation was used, finely distributed rod-like MoO_3 nanoparticles with shortened width and length was obtained. TEM analysis further confirmed the dispersed growth of rod-like MoO_3 crystallites (Fig. 5c and d) with the approximate diameter of 50–70 nm and the approximate length of 200–400 nm. HR-TEM analysis (Fig. 5e) shows the clear lattice fringes of crystallographic planes corresponding to the hexagonal phase. Furthermore, obtained crystalline dotted SAED patterns (Fig. 5f) support the formation of hexagonal MoO_3 nanoparticles. Although crystalline phase change cannot be observed by using different synthesis methodologies, it reflects on the change on crystallite sizes, which critically influence their surface area and provide a potential requirement in catalysis reaction.

The specific surface areas of the prepared MoO_3 nanoparticles were presented as Brunauer–Emmett–Teller (BET) surface areas in Fig. 6. The surface area measurements gave the surface areas of 0.43 $m^2 g^{-1}$, 1.15 $m^2 g^{-1}$, and 4.85 $m^2 g^{-1}$ for the MoO_3 synthesized in thermal, microwave, and sonochemical methods, respectively. Comparatively, MoO_3 obtained from sonochemical method shows a higher surface area than the other methods. This result is consistent with the findings in crystallite size changes.

3.2. Catalytic ozonation of orange II dye

The catalytic activities of the prepared MoO_3 nanoparticles were evaluated for the catalytic ozonation of orange II dye in aqueous environment. The color removal rate of orange II dye as a function of reaction time is shown in Fig. 7. For comparison, the color removal experiment in the absence of MoO_3 catalyst was also conducted, where the color removal increases with increasing reaction time and reaches around 50%. In general, the color removal is attributed to the breaking of azo bond present in the dye molecule. As the results of direct ozonation and hydroxyl radicals formed from ozone decomposition [41], the oxidation of dye molecules takes place. In addition, Fig. 7 also shows the color removal of orange II in the presence of ozone and MoO_3 nanocatalyst prepared by thermal, microwave, and sonochemical methods, respectively. It is clearly seen in Fig. 7 that color removal is completely achieved in the similar reaction time of 30 min in all MoO_3 catalyzed ozonation experiments. MoO_3 nanoparticles obtained from thermal and microwave method can initiate the catalytic degradation reactions and result in complete color removals in 30 min and 25 min, respectively. Whereas in the case of sonochemical MoO_3 catalyzed experiments, a very fast degradation was achieved and complete color removal was

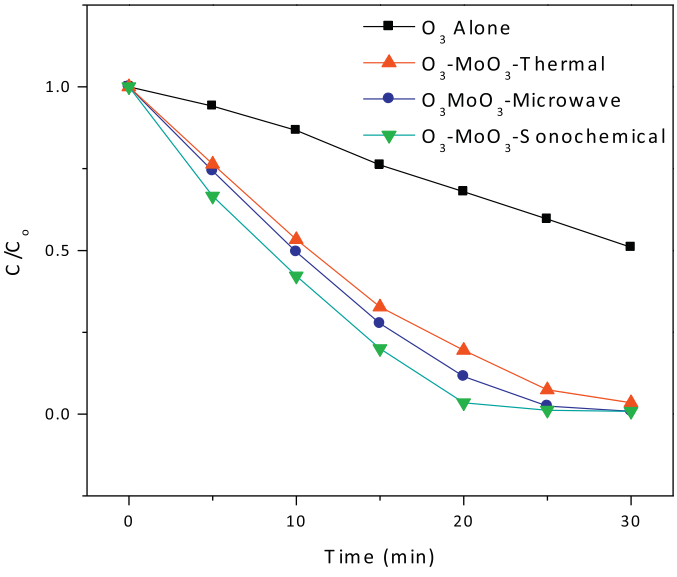

Fig. 7. Color removal plot for the degradation of orange II dye in absence and presence of MoO_3 nanoparticles prepared in different methods.

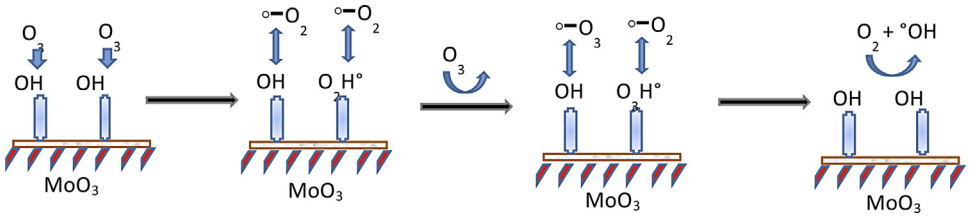

Fig. 9. Hydroxyl radical production by the interaction of ozone with MoO_3.

brought out in a shorter time, 20 min. The color removal in the presence of catalyst without ozone was also carried out as separate experiment and insignificant degradation was noticed. The degradation kinetics of the orange II dye was also investigated by fitting the experimental data with Langmuir–Hinshelwood model. Fig. 8 shows the plot of $-\ln(C/C_0)$ against time 't' which furnished a straight line fit with the correlation coefficient close to unity ($r^2 = 0.99$), indicated that the kinetics of the degradation reaction was followed first-order rate law and the apparent first order rate constants were calculated from the slope of the plot. The degradation rate constant values of $2.775 \times 10^{-4}\,s^{-1}$, $1.160 \times 10^{-3}\,s^{-1}$, $1.323 \times 10^{-3}\,s^{-1}$, and $1.656 \times 10^{-3}\,s^{-1}$ were obtained for without catalyst and with MoO_3 catalyst prepared in thermal, microwave, and sonochemical method, respectively. The degradation kinetic rates increased when MoO_3 catalysts were used and this may be attributed to the enhanced generation of hydroxyl radicals on the catalyst surface to initiate and promote the degradation of orange II [42]. The quantity of hydroxyl radical generation and dye adsorption depends on the number of active sites and oxygen vacancies present on the catalyst surface, which greatly depends on the adopted synthetic procedure of the catalyst. Although we use the similar starting materials for the preparation of different MoO_3 catalysts, sonochemical method can produce the MoO_3 nanoparticles with smaller size and high surface area than the other thermal and microwave methods. In addition, extreme sonochemical conditions would generate higher number of active sites accompanied by the production of more surface area of the catalyst for effective dye interaction. Therefore, ozone molecules could combine with the surface OH functional groups on the catalyst and accelerate the reactive radical formation that enhances the degradation rate [43]. The pathway of hydroxyl radical production was proposed by the interaction of ozone with the MoO_3 catalyst as shown in Fig. 9.

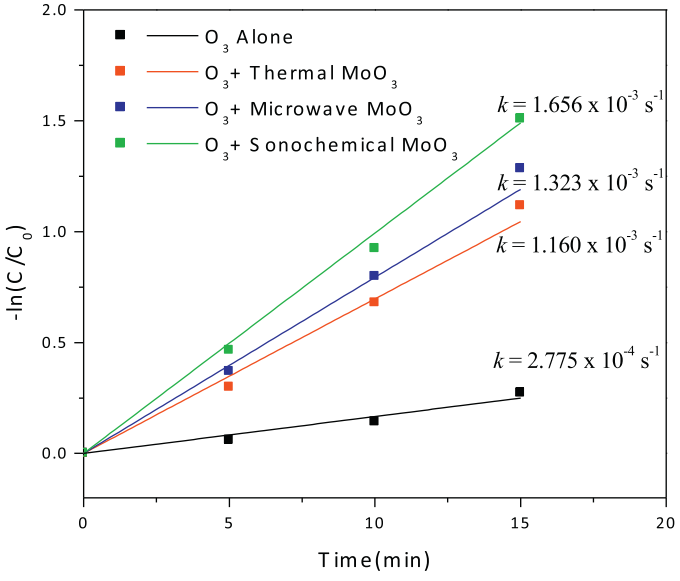

Fig. 8. Plot of $-\ln(C/C_0)$ vs. time for the degradation of orange II dye in absence and presence of MoO_3 nanoparticles prepared in different methods.

4. Conclusions

In this study, we have effectively synthesized MoO_3 nanoparticles using thermal, microwave, and sonochemical methods. Their catalytic ozonation abilities were successfully demonstrated for the degradation of an azo dye orange II. The effects of synthesis methodology on the physicochemical properties of the synthesized nanoparticles were analyzed and discussed. Hexagonal rod-shaped MoO_3 nanoparticles were obtained in all procedures as used and the change in methodology would not bring out any change in crystalline phase changes, but change in crystallite size has been substantially noticed. The catalytic ozonation experiments indicate that MoO_3 nanoparticles prepared in sonochemical method gave higher color removal and degradation rate than the microwave MoO_3, thermal MoO_3, and ozone alone. Nearly 6 fold enhancements in degradation rate was observed when using sonochemical MoO_3 nanoparticles while thermal and microwave produce nearly 4 and 4.7 fold enhancement than ozonation without catalyst. The higher degradation rate may be attributed to the improved generation of active radicals on the MoO_3 catalyst surface and also the enhanced surface area of sonochemical MoO_3 with higher number of active sites can provide effective dye interaction for the enhanced degradation rate of dyes.

Acknowledgements

The authors wish to thank for the financial support by the National Science Council (NSC) in Taiwan under the contract number of 100-2632-E-35-001-MY3. The support in providing the fabrication and measurement facilities from the Precision Instrument Support Center of Feng Chia University is also acknowledged.

References

[1] J.L.G. Fierro, Metal Oxides: Chemistry and Applications, CRC Press, Florida, 2006.
[2] A.R. José, F.G. Marcos, Synthesis, Properties, and Applications of Oxide Nanomaterials, New Jersey, Willey, 2007.
[3] G.R. Patzke, F. Krumeich, R. Nesper, Oxidic nanotubes and nanorods – anisotropic modules for a future nanotechnology, Angew. Chem. Int. Ed. 41 (2002) 2446–2461.
[4] J.N. Yao, K. Hashimoro, A. Fujishima, Photochromism induced in an electrolytically pretreated MoO_3 thin film by visible light, Nature 355 (1992) 624–626.
[5] J.F. Wang, K.C. Rose, C.M. Lieber, Load-independent friction: MoO_3 nanocrystal lubricants, J. Phys. Chem. B 103 (1999) 8405–8409.
[6] F. Hamelmann, K. Gesheva, T. Ivanova, A. Szekeres, M. Abroshev, U. Heinzmann, Optical and electrochromic characterization of multilayered mixed metal oxide thin films, J. Optoelectron. Adv. Mater. 7 (2005) 393–399.
[7] C.V. Krishnan, J. Chen, C. Burger, B. Chu, Polymer-assisted growth of molybdenum oxide whiskers via a sonochemical process, J. Phys. Chem. B 110 (2006) 20182–20188.
[8] J.W. Rabalais, R.J. Colton, A.M. Guzman, Trapped electrons in substoichiometric MoO_3 observed by X-ray electron spectroscopy, Chem. Phys. Lett. 29 (1974) 131–133.

[9] C.A. Ellefson, O. Marin-Flores, S. Ha, M.G. Norton, Synthesis and applications of molybdenum (IV) oxide, J. Mater. Sci. 47 (2012) 2057–2071.
[10] Y. Shi, B. Guo, S.A. Corr, Q. Shi, Y.S. Hu, K.R. Heier, L. Chen, R. Seshadri, G.D. Stucky, Ordered mesoporous metallic MoO_2 materials with highly reversible lithium storage capacity, Nano Lett. 9 (2009) 4215–4220.
[11] D.P. Debecker, M. Stoyanova, U. Rodemerck, E.M. Gaigneaux, Facile preparation of MoO_3/SiO_2–Al_2O_3 olefin metathesis catalysts by thermal spreading, Stud. Surf. Sci. Catal. 175 (2010) 581–585.
[12] Y. Chen, C. Lu, L. Xu, Y. Ma, W. Hou, J. Zhu, Single-crystalline orthorhombic molybdenum oxide nanobelts: synthesis and photocatalytic properties, Cryst. Eng. Comm. 12 (2010) 3740–3747.
[13] A. Chithambararaj, A.C. Bose, Investigation on structural, thermal, optical and sensing properties of meta-stable hexagonal MoO_3 nanocrystals of one dimensional structure, Beilstein J. Nanotechnol. 2 (2011) 585–592.
[14] A. Ganguly, R. George, Synthesis, characterization and gas sensitivity of MoO_3 nanoparticles, Bull. Mater. Sci. 30 (2007) 183–185.
[15] W. Dong, H. Huang, Y. Zhu, X. Li, X. Wang, C. Li, B. Chen, G. Wang, Z. Shi, Room-temperature solution synthesis of Ag nanoparticle functionalized molybdenum oxide nanowires and their catalytic applications, Nanotechnology 23 (2012) 425602.
[16] L. Zhou, L. Yang, P. Yuan, J. Zou, Y. Wu, C. Yu, α-MoO_3 nanobelts: a high performance cathode material for lithium ion batteries, J. Phys. Chem. C 114 (2010) 21868–21872.
[17] A.M. Hashema, H. Groult, A. Mauger, K. Zaghib, C.M. Julien, Electrochemical properties of nanofibers α-MoO_3 as cathode materials for Li batteries, J. Power Sources 219 (2012) 126–132.
[18] Q. Xia, H. Zhao, Z. Du, J. Wang, T. Zhang, J. Wang, P. Lv, Synthesis and electrochemical properties of MoO_3/C composite as anode material for lithium-ion batteries, J. Power Sources 226 (2013) 107–111.
[19] F.J. Zhang, D.W. Zhao, Z.L. Zhuo, H. Wang, Z. Xu, Y.S. Wang, Inverted small molecule organic solar cells with Ca modified ITO as cathode and MoO_3 modified Ag as anode, Sol. Energy Mater. Sol. Cells 94 (2010) 2416–2421.
[20] F. Cheng, G. Fang, X. Fan, N. Liu, N. Sun, P. Qin, Q. Zheng, J. Wan, X. Zhao, Enhancing the short-circuit current and efficiency of organic solar cells using MoO_3 and CuPc as buffer layers, Sol. Energy Mater. Sol. Cells 95 (2011) 2914–2919.
[21] K. Bange, Colouration of tungsten oxide films: a model for optically active coatings, Sol. Energy Mater. Sol. Cells 58 (1999) 1–131.
[22] X.W. Lou, H.C. Zeng, Hydrothermal synthesis of α-MoO_3 nanorods via acidification of ammonium heptamolybdate tetrahydrate, Chem. Mater. 14 (2002) 4781–4789.
[23] P. Badica, Preparation through the vapor transport and growth mechanism of the first-order hierarchical structures of MoO_3 belts on sillimanite fibers, Cryst. Growth Des. 7 (2007) 794–801.
[24] N.A. Chernova, M. Roppolo, A.C. Dillon, M.S. Whittingham, Layered vanadium and molybdenum oxides: batteries and electrochromics, J. Mater. Chem. 19 (2009) 2526–2552.
[25] J. Song, X. Ni, D. Zhang, H. Zheng, Fabrication and photoluminescence properties of hexagonal MoO_3 rods, Solid State Sci. 8 (2006) 1164–1167.
[26] J. Song, X. Ni, L. Gao, L. Zheng, Synthesis of metastable h-MoO_3 by simple chemical precipitation, Mater. Chem. Phy. 102 (2007) 245–248.
[27] S.S. Mahajan, S.H. Mujawar, P.S. Shinde, A.I. Inamdar, P.S. Patil, Concentration dependent structural, optical and electrochromic properties of MoO_3 thin films, Int. J. Electrochem. Sci. 3 (2008) 953–960.
[28] A. Chithambararaj, A.C. Bose, Hydrothermal synthesis of hexagonal and orthorhombic MoO_3 nanoparticles, J. Alloys Compd. 509 (2011) 8105–8110.
[29] L.P.M. Cai, X. Rao Zheng, Morphology-controlled flame synthesis of single, branched, and flower-like α-MoO_3 nanobelt arrays, Nano Lett. 11 (2011) 872–877.
[30] M.B. Rahmani, S.H. Keshmiri, J. Yu, A.Z. Sadek, L. Al-Mashat, A. Moafi, K. Latham, Y.X. Li, W. Wlodarski, K. Kalantar-zadeh, Gas sensing properties of thermally evaporated lamellar MoO_3, Sens. Actuators B 145 (2010) 13–19.
[31] C. Imawan, H. Steffes, F. Solzbacher, E. Obermeier, A new method for the preparation of sputtered MoO_3 multilayers for the application in gas sensors, Sens. Actuators B 78 (2001) 119–125.
[32] E. Comini, L. Yubao, Y. Brando, G. Sberveglieri, Gas sensing properties of MoO_3 nanorods to CO and CH_3OH, Chem. Phys. Lett. 2005 (2005) 368–371.
[33] L. Zheng, Y. Xu, D. Jin, Y. Xie, Novel metastable hexagonal MoO_3 nanobelts: synthesis, photochromic, and electrochromic properties, Chem. Mater. 21 (2009) 5681–5690.
[34] W. Dong, Z. Shi, J. Ma, C. Hou, Q. Wan, S. Feng, A. Cogbill, Z.R. Tian, One-pot redox syntheses of heteronanostructures of Ag nanoparticles on MoO3 nanofibers, J. Phys. Chem. B 110 (2006) 5845–5848.
[35] Y. Li, Y. Bando, Quasi-aligned MoO_3 nanotubes grown on Ta substrate, Chem. Phys. Lett. 364 (2002) 484–488.
[36] A. Chithambararaj, A.C. Bose, Microwave assisted ultra fast synthesis of 1-D molybdenum oxide nanocrystals: structural and electrical studies, Adv. Mater. Res. 488–489 (2012) 940–944.
[37] D.D. Yao, J.Z. Ou, K. Latham, J. Zhuiykov, A.P. O'Mullane, K. Kalantar-zadeh, Electrodeposited α- and β-phase MoO_3 films and investigation of their gasochromic properties, Cryst. Growth Des. 12 (2012) 1865–1870.
[38] S. Baia, S. Chena, L. Chenb, K. Zhanga, R. Luoa, D. Li, C. Liu, Ultrasonic synthesis of MoO_3 nanorods and their gas sensing properties, Sens. Actuators B. 174 (2012) 51–58.
[39] A. Bouzidi, N. Benramdane, H. Tabet-Derraz, C. Mathieu, B. Khelifa, R. Desfeux, Effect of substrate temperature on the structural and optical properties of MoO_3 thin films prepared by spray pyrolysis technique, Mater Sci. Eng. B 97 (2003) 5–8.
[40] B. Jin, H. Bang, K.S. Suslick, Applications of ultrasound to the synthesis of nanostructured materials, Adv. Mater. 22 (2010) 1039–1059.
[41] B. Kasprzyk-Hordern, M. Ziolek, J. Nawrocki, Catalytic ozonation and methods of enhancing molecular ozone reactions in water treatment, Appl. Catal. B Environ. 46 (2003) 639–669.
[42] R. Amutha, M. Sillanpää, G.J. Lee, J.C. Lin, C.K. Yang, J.J. Wu, Catalytic ozonation of 2-ethoxy ethyl acetate using mesoporousnickel oxalates, Catal. Commun. 43 (2014) 88–92.
[43] G. Moussavi, M. Mahmoudi, Degradation and biodegradability improvement of the reactive red 198 azo dyeusing catalytic ozonation with MgO nanocrystals, Chem. Eng. J. 152 (2009) 1–7.